Research Square

Preprints are preliminary reports that have not undergone peer review.
They should not be considered conclusive, used to inform clinical practice,
or referenced by the media as validated information.

Experimental and Theoretical Quantification of Direct 20 keV Electron Beam Induced Damage to Aqueous DNA

Nazifa Tabassum
University of Missouri
Rachel L. Johnson
University of Missouri
Cecil D. Terrell III
University of Missouri
Peter V. Cornish
University of Missouri
David Stalla
University of Missouri
Gavin M. King
University of Missouri
Kurt R. Brorsen
kbrorsen@missouri.edu
University of Missouri

Article

Keywords: DNA damage, Ice lithography, keV electrons, Aqueous DNA

Posted Date: November 19th, 2026

DOI: https://doi.org/10.21203/rs.3.rs-11554337/v1

License: This work is licensed under a Creative Commons Attribution 4.0 International License.
Read Full License

Additional Declarations: No competing interests reported.

Experimental and Theoretical Quantification of Direct 20 keV Electron Beam Induced Damage to Aqueous DNA

N. Tabassum[1], R. L. Johnson[1,2], C. D. Terrell III[3], P. V. Cornish[3], D. Stalla[4], G. M. King*[2,3,5], K. R. Brorsen*[1]

[1]Department of Chemistry, University of Missouri, Columbia, MO 65211, USA. [2]Department of Physics and Astronomy, University of Missouri, Columbia, MO 65211, USA. [3]Department of Biochemistry, University of Missouri, Columbia, MO 65211, USA. [4]Electron Microscopy Core Facility, University of Missouri, Columbia, MO 65211, USA. [5]Materials Science and Engineering Institute, University of Missouri, Columbia, MO 65211, USA.

*Corresponding authors: kinggm@missouri.edu, kbrorsen@missouri.edu

Keywords: DNA damage, Ice lithography, keV electrons, Aqueous DNA

Abstract

Understanding electron irradiation-induced biomolecule damage at the mechanistic level is critical to diverse fields ranging from fundamental biophysics to radiotherapy. Comprehending electron-soft matter interactions is also relevant to advanced electron microscopy-based nanofabrication technologies like ice lithography where keV electrons are employed to directly functionalize biomaterials using solid phase condensed gases as resist. In this study, we investigate the damage caused to DNA by electrons in an energy regime relevant to high resolution electron beam lithography. We used aqueous plasmid DNA (4,361 base pairs, pBR322) irradiated with 20 keV electrons from an environmental scanning electron microscope as a test system. The progression from a supercoiled state to open circle to linear plasmid conformers was quantified via gel electrophoresis. We complemented the experiments with Geant4-DNA Monte Carlo track structure simulations. These calculations successfully reproduced the main features of the conformational abundances with only slight underestimation of the overall macromolecular damage and provide insight into the important role of the medium in which the DNA is suspended. This report presents a first assessment of direct ~10 keV-scale electron irradiation on aqueous DNA and represents a step towards characterizing biomolecular damage induced during high precision functionalization via ice lithography.

1. Introduction

Biological science and technology have advanced through the development and application of high-resolution patterning techniques such as electron beam (e-beam) lithography. Exploiting the core functionality of a scanning electron microscope (SEM), this well-established fabrication method enables direct functionalization of substrate surfaces at the nanometer length scale. E-beam lithography is used to realize a variety of devices including high density neural probes for biomedical applications, plasmonic nanostructures for biophysical sensing, and nanopores for high-throughput macromolecular characterization.[1–5] In typical applications, lithographic patterning is performed on substrate surfaces which are then placed in contact with cells or tissues or employed as a platform for *in vitro* characterization experiments.

Can biomaterials be patterned directly via e-beam lithography? Such a capability would be a paradigm shift for the field and portends fully integrated biosensors and devices, but key steps of the e-beam lithography process present significant challenges. For example, the (*i*) application of polymer resist dispersed in liquid phase solvent, (*ii*) heating to drive out the solvent, and (*iii*) post exposure resist development, are all steps which can denature, damage, or destroy biomolecules.

By using a variation of e-beam lithography that replaces conventional liquid phase resists with solid phase condensed gases,[6,7] researchers have recently shown that sub-100 nm patterns can be written directly on organisms (tardigrades) and on isolated biological membranes (purple membrane patches from *H. salinarum*).[8,9] Though successfully side-stepping the deleterious effects of conventional liquid phase resists, these ice lithography demonstrations did not rigorously assess biomolecule damage resulting from the lithographic patterning. Independent of the resist employed, some amount of radiation damage would generally be expected from e-beam writing, an immutable component of the e-beam lithography process.

We sought to quantify e-beam-induced damage in the context of high-resolution functionalization of biomaterial. To gain traction, we focus on a simple model system – purified plasmid DNA commonly used in molecular biology and genetics – and subject the biological macromolecules in aqueous system to direct e-beam irradiation in an energy range (20 kV) typically employed in e-beam lithography (**Fig. 1**). The low vacuum requirements (operation at pressures >1000 Pa) coupled with sample temperature and humidity control of an environmental SEM allowed aqueous fluid conditions to be maintained throughout the irradiation process.[10] In the context of oncology and other fields, previous reports have explored the effects of electron irradiation on DNA using lower (≤4 keV) and sustainably higher energy (1 – 250 MeV) electrons.[11–15] The direct irradiation by lower energy beams have generally required high vacuum conditions (<0.01 Pa) where the DNA is dried on a surface,[11,12] a process that itself can damage biomolecules.[16] A handful of aqueous 30 keV studies have been reported using a customized silicon nitride membrane window fixture separating the SEM chamber from the liquid phase solution.[17,18] Passing through a solid-state window lowers the e-beam flux and causes undue inelastic scattering prior to interacting with the DNA solution.[17,18] Although the present configuration avoids interference of a solid window, some amount of electron beam broadening is associated with the scattering in the chamber. Simulations were carried out using DTSA-II (accessed from DTSA), a software package maintaned by NIST. Approximately 80% of the recorded electron counts were distributed within

a radial distance of 1 mm. (**Supplementary Fig. S1**) Corresponding to a 2 mm diameter within the ~5 mm wide liquid droplet, it implies that majority recorded electrons still reach the sample.

Radiation damage can occur by either direct e-beam/DNA interactions or by indirect action of reactive species produced from the irradiated medium (typically water) surrounding the DNA.[19–21] As ionizing radiation interacts with the fluid medium, electrons are solvated and radicals (primarily •OH, •H, and e_{aq}^{-1}) are produced. Hydroxyl radicals are the most significant because they can remove hydrogen atoms from the sugars or oxidize nucleobases that can result in cleavage of the sugar-phosphate backbone.[22,23] Nucleic acid damage is often studied using plasmids and caused by strand breaks (SB) of the sugar-phosphate backbone. Prior to external perturbation, plasmid DNA exists primarily in a compact, topologically constrained supercoiled (SC) state. In addition to the SC state, plasmid DNA can also exist in a relaxed, open circle (OC) form, as well as in a linear (L) state (**Fig. 1B-D**).[24,25] Exposure to e-beam irradiation causes single strand breaks (SSB) in the DNA backbone, thereby converting the SC configuration to OC. Upon further exposure to the e-beam, OC DNA can be cut again, causing a double strand break (DSB). The L configuration can be induced if two or more breaks occur on opposing strands within ~10 base pairs of each other. Gel electrophoresis is a well-established technique that provides quantitative assessment of the irradiation-induced DNA damage.[26,27]

Theoretical models provide insights that complement experimental biomolecular damage measurements. Monte Carlo track-structure simulations have been developed over several decades to study radiation effects on biological media.[28–41] Of particular relevance, Geant4-DNA - originally developed within the high energy particle physics and radiopharmaceuticals community - is an open-source package for simulation of radiation track structures that can simultaneously model direct and indirect DNA damage modes in liquid water.[29,40–49] Hence, Geant4-DNA is well suited for quantitative comparison with our experiments.

In this work, we investigated the damage caused to plasmid DNA in solution by 20 keV electrons using a joint experimental-computational approach. Direct irradiation of the DNA in a bulk aqueous system was achieved without the beam passing through a solid-state window by employing an environmental SEM under conditions that maintained a stable liquid phase. The resulting damage was analyzed by exploiting the differing electrophoretic mobilities of the supercoiled, circular, and linear DNA conformations. Simulations were carried out using Geant4-DNA with input parameters mimicking the experimental conditions. Taken all together, this work provides a mechanistic understanding of direct damage to aqueous DNA in an energy regime relevant to electron beam lithography and highlights the role that sample conditions play in the beam-induced macromolecular structural changes.

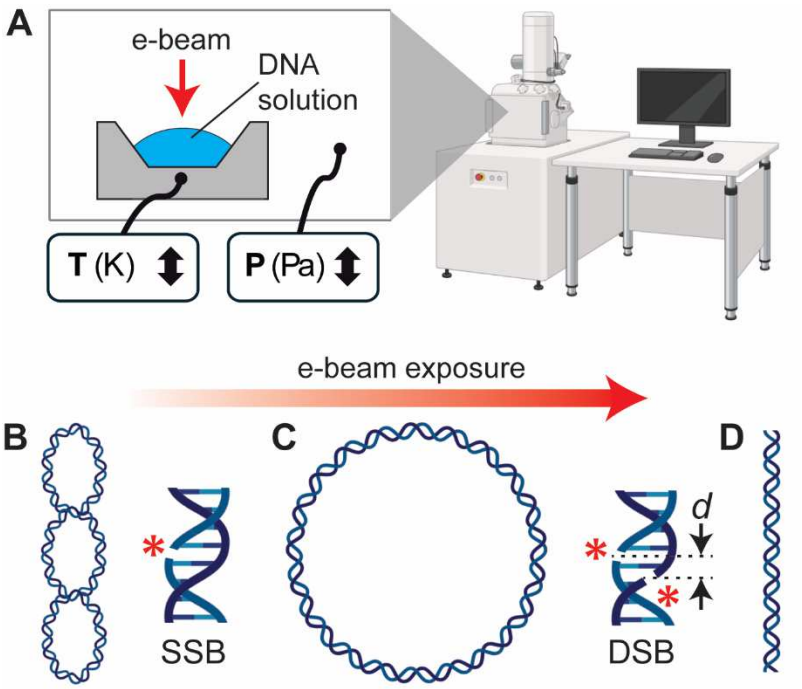


Figure 1. Experimental Overview. (**A**) An environmental SEM is employed to irradiate DNA using temperature, *T*, and pressure, *P*, conditions that maintain liquid phase water. (**B**) Cartoon showing supercoiled configuration of the plasmid DNA starting material. SSBs are formed upon e-beam exposure, leading to (**C**) open circle DNA. (**D**) Upon further irradiation, linear DNA forms via DBSs (the result of SSBs occurring within a distance d ≤ 10 base pairs). Figure drafted with assistance from BioRender (https://www.biorender.com/).

2. Methodology

2.1 Experimental Methods

We employed 4,361 bp plasmid DNA (pBR322, ThermoScientific) in aqueous buffer solution (10 mM Tris-HCl, pH 7.6, 1 mM EDTA) at a stock concentration of 500 ng/μL. After e-beam irradiation samples were dyed (6x TriTrack DNA, ethidium bromide, ThermoScientific) and gel electrophoresis was performed using a 0.8% agarose matrix in tris-borate-EDTA buffer with a potential of 60 V/m and a current of 30 mA. DNA samples were visualized with ultraviolet light (UV visualizer, BioRad) and quantified using software (ImageJ[50]). A DNA ladder was purchased (ThermoScientific).

DNA dissolved in water was irradiated using an environmental scanning electron microscope (FEI Quanta 600F). Volumes (~5 μL) of DNA at stock concentration were injected onto a temperature controlled sample holder **(Fig. 1A)** in a low vacuum environment and subjected to a 20 keV electron beam using a beam current of ~2 nA. Conditions were chosen to maintain stable liquid phase water (~14 °C, ~1700 Pa) along with an equilibration time of 5 minutes each time after loading the sample. After centering the imaging field on the fluid droplet, samples were irradiated via raster scanning (250 μm × 216 μm area; 1024 pixels × 884 pixels; pixel dwell time = 1 μs). The dose delivered was controlled by varying the total irradiation time, calculated through the constant dose rate of 0.0037 μC/cm^2/s. After irradiation, samples were extracted

from the environmental SEM via a pipette, analyzed in a spectrophotometer (NanoDrop 2000c, ThermoScientific) and diluted to specific concentrations (~20 ng/μL) for gel electrophoresis analysis.

2.2 Simulation Methods

The Geant4-DNA (v11.2.2) software was used to simulate the experimental electron irradiation process and subsequent plasmid damage. Geant4-DNA explicitly considers three stages of the radiation process in liquid water. The first stage is the physical stage**,** where elastic scattering, ionization, and electronic excitation of primary electrons are considered. The next step is the physico-chemical stage**,** where the electrons are solvated and radicals are formed. The final stage is the chemical stage**,** where the reactive species diffuse and interact with the target DNA to induce strand breaks. In this study, the works of D. Kondo et al.[29] and Ramos-Mendez et al.[46] in Geant4-DNA were adapted with parameters modified to be appropriate for the experimental system. A set of reactions involving primarily •OH, •H, e_{aq}^{-1} and the products resulting from their reactions are included in the chemical stage. To match the experimental conditions, reactions involving scavengers were omitted.

Molecules were constructed following a previous study with a smaller plasmid (2,686 bp).[29,47] The existing coordinate file of the smaller plasmid was extended to 4,361 bp file and visualized using Python and VMD[51] (accessed through VMD). The target plasmid was represented via a coarse-grained model[52] that treats DNA base pairs as semi-spheres with specified center of mass coordinates. To calculate the full DNA structure, the first sphere is placed, then a second pair is placed with a fixed angular rotation and a variable vertical distance between two nucleotides up to 0.34 nm. After placing the first bp sphere, the next bp is positioned in the plane perpendicular to the local tangent of the backbone skeleton. This local tangent of the backbone skeleton is defined by the direction between neighboring vertices. Thus, lateral bending is inherited from the skeleton. The bp tilts with the direction of the tangent and the helical twist of 36º is applied separately about the tangent. This process is continued for the full DNA structure and a file with the bp positions as cartesian (xyz) coordinates is obtained. The final pBR322 plasmid (**Supplementary Fig. S2**) was used for all simulations.

For each combination of irradiation time and plasmid concentration, we ran a simulation with the number of primary electrons and the radius of the water sphere encapsulating the DNA (**Supplementary Fig. S2**) as the two variable inputs. The number of irradiated electrons in the simulations was calculated to match experimental values using the irradiation time and the beam current (**Supplementary Table 1**). For all simulations, the radius of the surrounding water sphere was calculated to match the experimental plasmid concentration. Other parameters including plasmid geometry, electron beam energy, position of the electron source, the physics model, and the chemistry model were kept constant for all systems.

For each plasmid concentration and electron dose combination, the simulation system containing the single target plasmid surrounded by the water sphere is irradiated by the required number of electrons. Each electron irradiation is defined as an event. The outcome of each event is assumed to be independent of other events in all Geant4-DNA codes.[29] After the simulation is completed, the output files are analyzed to determine the number of different plasmid conformers. A direct SSB was defined to occur if 17.5 eV of energy was deposited in the sugar-phosphate region (r ~ 0.6 nm). Indirect SSBs were determined during the chemical stage when the water radiolysis

products reacted with the DNAs. According to the reaction scheme shown by Kondo et al.,[29] •OH and H• produce intermediate products OHDNA and HDNA, respectively, by reacting with DNA. However, not all interactions between radicals and DNA will result in an SB. Therefore, the previous studies introduced SB efficiency terms λ_{OH} and λ_H, which defines the probability of a OHDNA or HDNA producing an indirect SB. These efficiencies were calibrated using the Nelder-Mead (NM) optimization algorithm,[53] a method that iteratively calculates λ_{OH} and λ_H using their respective trial values. This method works by comparing simulated results with experimental reference data until the differences between them is minimized using the following function:

$$F(\lambda_{\mathrm{OH}}, \lambda_{\mathrm{H}}) = \int_{x_f}^{x_i} |\gamma_{\mathrm{ref}}(x) - (\lambda_{\mathrm{OH}}\mathrm{OHDNA}(x) + (\lambda_{\mathrm{H}}\mathrm{HDNA}(x))| dx, \quad (1)$$

where γ_{ref} is the experimental reference value, and OHDNA and HDNA are the simulated values of product yields of the corresponding reactions. The integration limits x_i and x_f vary with the simulation setup. After optimization, the SB yields were calculated using the formula shown below:[29]

$$\mathrm{SB} = \mathrm{OHDNA} \times \lambda_{\mathrm{OH}} + \mathrm{HDNA} \times \lambda_{\mathrm{H.}} \quad (2)$$

A DSB was defined when two SSBs occurred within a distance of ≤ 10 bp along the DNA backbone. The percentage of each conformation at the end of the simulation was calculated with respect to the total number of plasmids. These percentages were compared with the values obtained experimentally.

3. Results and Discussion

3.1 Experimental Results

3.1.1 Irradiation of plasmids and dose dependence of DNA damage: We investigated the damage caused to DNA in solution by increasing the dose of 20 keV electrons. Under the constant beam current used in the environmental SEM, the delivered dose was controlled by varying the irradiation time (**Supplementary Table 1**). **Fig. 2a** shows representative data after irradiation from 0 s to 900 s, corresponding to a maximum dose of 3.3 mC/cm^2.

A sample from the original stock solution (SC – 95.2%, OC – 4.8%, L - 0%, see **Supplementary Fig. S3**) was placed inside the vacuum for the duration of the experiment, but not irradiated. This non-irradiated sample then contained 93.7% SC and 6.3% OC DNA (**Fig. 2a/Supplementary Figure S4, lane 1**), with no measurable L fraction. This was used as control sample for the dose variation experiments.

Upon irradiation, damage was already evident after the shortest irradiation time (5 s) with quantitative analysis showing the percentage of OC increasing to 19.2% and the emergence of L bands with 0.4% abundance. This trend continued until undamaged SC reached an abundance of 13.6% along with significant increase in damage with a total of 86.4% (84.1% OC and 2.3% L) at the longest irradiation time 900 s. (**Supplementary Fig. S5**) A transition of an SC-dominated system to an OC-dominated system is seen in the dose range of ~1 mC/cm^2.

The abundances of each conformation for the complete range of radiation dose were plotted versus the irradiation time and fit to the McMahon model[54] (**Fig. 2b**) which was developed to represent the results of plasmid damage by irradiation. In the model, the dose, *D*, dependent amount of each conformer is given by,

$$SC\,(D) = S_o e^{-(\mu D + \phi D)}, \quad (3)$$

$$OC\,(D) = e^{-\phi D}\left[e^{-\frac{1}{2}\mu^2 \rho D^2}(S_o + C_o) - S_o e^{-\mu D}\right], \quad (4)$$

and

$$L\,(D) = 1 - (S_o + C_o)e^{-\left(\phi D + \frac{1}{2}\mu^2 \rho D^2\right)}. \quad (5)$$

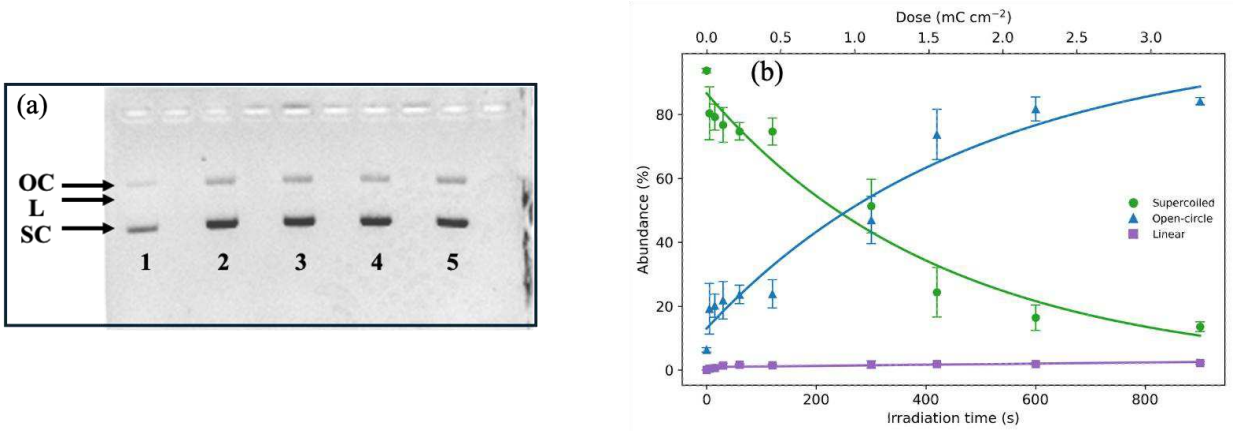


Figure 2: (a) Representative gel image of pBR322 plasmid irradiated with 20 keV electrons for increasing times. Lanes correspond to increasing irradiation time (Lanes: 1: 0 s, 2: 5 s, 3: 15 s, 4: 30 s, 5: 60 s). All samples were diluted to ~20 ng/μL prior to loading in gels. The three conformer bands SC, OC and L are indicated. The gel image is cropped. The uncropped image is provided in **Supplementary Figure S4**. (b) Experimentally measured abundances of the SC, OC, and L conformers as a function of irradiation time, fitted to the McMahon model (Solid line). The points are the mean of three independent irradiation experiments and error bars denote ±1 standard deviation. The top axis gives the corresponding dose.

In these equations, the obtained SC, OC, and L percentages are fitted and average yield of SSBs and DSBs per plasmid per unit of dose is obtained. S_o and C_o are SC and OC proportions at zero dose. In our case, these values are 93.7% and 6.3%, respectively. The parameter ρ is defined as the probability of a DSB formation from two SSBs within 10 base pairs on opposite strands. As the target plasmid is pBR322 (4361 bp), ρ = 10/4361 or 2.3 × 10^{-3}. Parameters μ and Φ define average yield of SSBs and DSBs per plasmid per unit of dose (seconds in this study), respectively. These parameters were calculated to be $\mu = 2.6 \times 10^{-3}\ s^{-1}$ and $\Phi = 3.7 \times 10^{-5}\ s^{-1}$, indicating that the SSB formation rate is much higher (70-fold) than the DSB formation rate under our experimental conditions.

3.1.2 Effect of DNA concentration

The effect of DNA concentration on the plasmid populations was examined at a fixed irradiation dose of 0.22 mC/cm^2. Quantitative analysis of the representative gel image (**Fig. 3a**) displays a decrease in the e-beam-induced damage with increasing DNA concentration from 50 to 500 ng/µL.

The average relative abundances of SC, OC, and L were quantified from the band intensities of the gel images (**Fig. 3a and Supplementary Fig S7**) and presented by a bar plot in **Fig. 3b**. With a two-tailed Student's t-test assuming equal variance (with $p < 0.05$ taken as statistically significant), the difference in abundances between two DNA concentrations was assessed for each conformer.

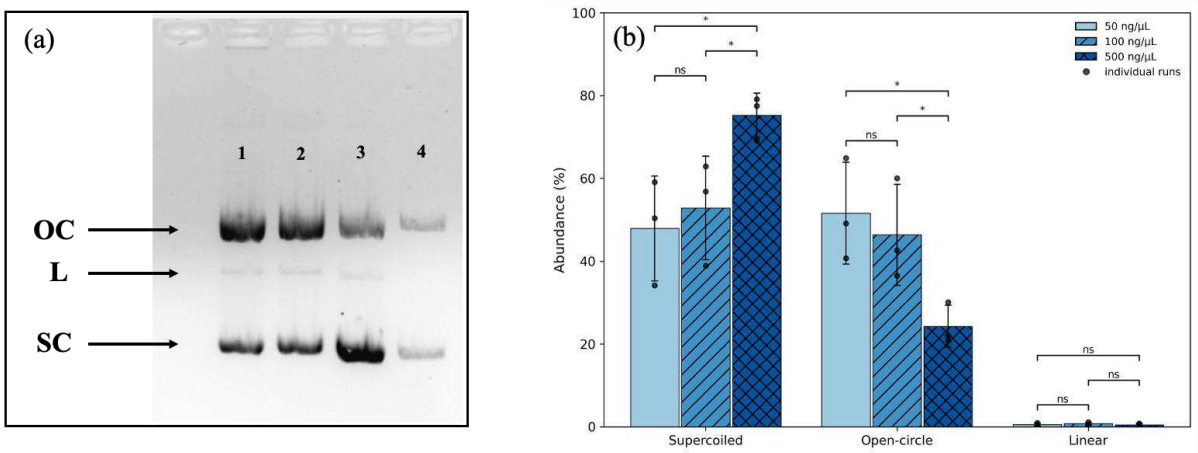


Figure 3: (a) Representative gel electrophoresis image (cropped) showing the damage produced by a fixed dose of 0.22 mC/cm^2 using 20 keV electrons at three DNA concentrations (from left to right, lanes: 1 - 50, 2 - 100, 3 - 500 ng/µL, 4 - control). The SC, OC and L bands are labelled. The gel image is cropped, the uncropped gel image is shown in **Supplementary Figure S6**. (b) Abundance of SC, OC and L conformers versus DNA concentration (50, 100, 500 ng/µL) after irradiation at a dose 0.22 mC/cm^2 with 20 keV electrons. Bars are means of three independent experiments. Significance between concentrations within each conformer: two-tailed Student's t-test (equal variance): * $p < 0.05$, ns ≥ 0.05.

At the lowest concentration studied (50 ng/µL), the irradiated plasmid population consisted of 47.9% SC, 51.6% OC, and 0.5% L DNA. The amount of damage decreased with increasing concentration. At the highest concentration (500 ng/µL), the OC fraction decreased to 24.3%, with a low fraction of L at 0.5%. Combining the total damaged DNA (OC + L) into a single percentage, the damage decreased from 52.1% at 50 ng/µL to 24.8% at 500 ng/µL, indicating an apparent protective effect of increasing DNA concentration when all other irradiation conditions are held constant. For the SC conformers, the abundance at 500 ng/µL differed significantly from that at both 50 and 100 ng/µL (Student's t-test, **Figure 3b,** $p = 0.026$ and 0.046, respectively). The OC conformer abundance at both 50 and 100 ng/µL also differed significantly from that at 500 ng/µL (Student's t-test, **Figure 3b**, $p = 0.024$ and 0.044, respectively). Differences between the two lower concentrations (50 vs 100 ng/µL) were not significant ($p = 0.65$ for SC and 0.63 for OC). No significant differences were found for the L conformer at any concentration indicating that this damage mode is negligible at this low dose range.

3.2 Simulation Results

3.2.1 Effect of Radiation Dose

The abundances of the different plasmid conformations with different radiation doses were determined from the MCTS simulations.

To replicate the no irradiation (0 s) condition, 100% of the simulated plasmid population in this condition was assumed to be in SC form. After 5 s of irradiation, the simulation predicted 89.5% SC, 10.3% OC and 0.2% L, compared with the experimentally measured 80.4% SC, 19.2% OC and 0.4% L. Similar to the experimental measurements, as the radiation dose increases, the abundance of SC decreased, OC gradually increased and the L fraction remained minor throughout. The model qualitatively reproduced the gradually increasing conversion of SC to OC, but the absolute OC percentage was slightly underestimated. The simulation predicted slightly lower values of L fractions than in the experimental measurements. The fractions from simulations were also fit to the McMahon model (**Fig. 4**) and were compared with the experimentally fitted results. Simulated abundances represent a single value per condition (averaged over primary particles), statistical error bars are therefore not shown.

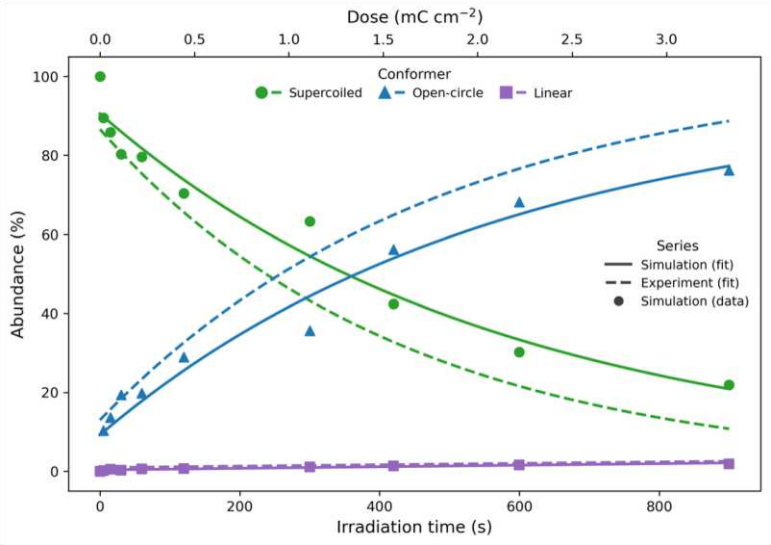


Figure 4: Abundances of the SC, OC, and L conformers as a function of irradiation time obtained from the Geant4-DNA simulations, fitted to the McMahon model and overlaid with the experimental fit results.

3.2.2 Effect of DNA Concentration

The effect of plasmid concentration on the conformer population was studied by changing the radius of the water sphere surrounding the target plasmid. The results of these simulations are presented in **Fig. 5**. With a one-sample t-test (with $p < 0.05$ taken as statistically significant), the differences between experimental (mean) and simulation values were assessed for each concentration and each conformer.

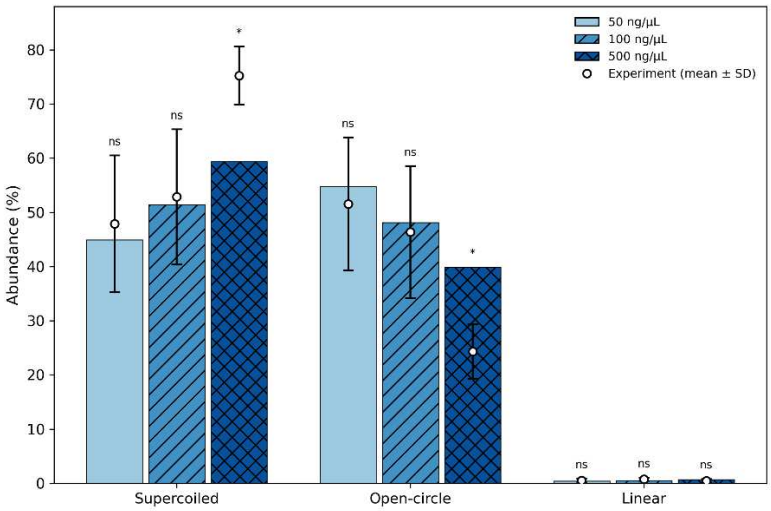


Figure 5: Bar plot showing simulated abundances of the SC, OC and L conformers as a function of DNA concentration (50, 100 and 500 ng/µL) at a fixed electron fluence equivalent to 60 s irradiation (0.22 mC cm^{-2}). The experimental results are overlaid as open circles (mean of three independent experiments), with error bars denoting ±1 standard deviation. Simulated values are single values per condition and therefore have no error bars. Two-tailed one-sample t-test (the three experimental replicates tested against the simulated value): * $p < 0.05$, ns = not significant. Simulation and experiment agree within error at 50 and 100 ng/µL, whereas at 500 ng/µL the simulation significantly underpredicts SC and over-predicts OC ($p = 0.036$ and $p = 0.033$, respectively).

At a concentration of 50 ng/µL, the simulation predicted 44.9% SC, 54.7% OC and 0.4% L compared with the experimental values of 47.9% SC and 51.6% OC and 0.5% L. The model overpredicted the damage at all concentrations, reaching a total simulated (OC+L) damage of 40.6% vs. 24.8% experimentally obtained total damage at 500 ng/µL. Only the values at 50 and 100 ng/µL fell within the experimental error. For both SC and OC conformers, the experimental and simulation abundance at 500 ng/µL concentration was found to be statistically significant. No significant differences were found for the L conformer at any concentration.

3.3 Discussion

As observed in the dose variation results, SC plasmids go through a progressive loss to produce relaxed OC plasmids accompanied by a smaller amount of L plasmids. 84.1% of OC and 2.3% of L population was obtained in this study at the longest dose, which indicates strand relaxation is identified as the dominant response over the investigated radiation dose range. This qualitative pattern is in good agreement with a closely related previous work by Hahn et al. on pUC19 in an aqueous environment irradiated by 30 keV electrons.[18] Their sample was irradiated through a 100 nm silicon nitride membrane in a high vacuum ($\leq 10^{-4}$ Pa), while the present study irradiated the sample directly and maintained the liquid sample state at low vacuum (~1700 Pa) condition. Despite having different sample geometry, plasmid size, and vacuum conditions, the comparison establishes the progression from an SC dominated system to an OC dominated system as an expected damage pattern for irradiation of aqueous DNA with keV energy electrons.

An important aspect of this study is the effect of aqueous surroundings around the plasmids. Hahn et al. studied the relation between SC loss and the amount of deposited energy in a targeted area including water within 7.5 nm of the sugar-phosphate region. Those results emphasized the fact that the damage cannot be solely attributed to the energy deposited within DNA itself.[17] The current study explores this direction in a different way by focusing on the radiolysis, diffusion and chemical reactions with DNA. Although no experiment was carried out in this study that can discriminate between direct and indirect contributions, the Geant4-DNA classifies each SB event according to mechanism. The model predicts approximately 98% of the SB events to be indirect, providing theoretical support to the fact that indirect damage typically dominates the total DNA damage yield in weakly scavenged aqueous plasmid system for low linear energy transfer (LET) radiation.[55] This result is consistent with the broad interpretation in Hahn et al.'s work about the significance of aqueous surroundings and the greater damage sensitivity found in the dry DNA study by Folkard et al. addressing the differences to additional processes involved with the surrounding medium.[11,18] We also mention that Small et al. compared DNA damage yields by 100-200 MeV electrons in dry and aqueous environments and determined that indirect effects caused ~99% of total DNA breaks, which is very close to our predicted value.[13]

For the low LET radiation such as electrons in this study, SSBs are generally found to be more frequent than DSB formation as a DSB requires either a single two-strand event or the accumulation of closely spaced (≤ 10 bp) breaks on opposite strands. This leads to most SSBs remaining as individual isolated SSBs, rendering DSB formation as a rare event. This fact is supported by our measured rates of formation (μ and ϕ values) which yield a DSB to SSB ratio of 0.014, referring to 1 DSB event per 70 SSB events. This 1:70 ratio can be compared with previously found 1:12 and 1:44 for Hahn et al.[18] and Small et al.,[13] respectively. The common indication from these values is that SSB events are more frequent than DSB. The numerical disagreement comes from the method used to acquire these yield values. The current study correlated dose with number of electrons instead of absorbed dose, per irradiated area which can also be used. The ratio value in this study was obtained from a combined fit of the conformer populations, while Hahn et al. determined the SSB yield from the initial survival curve and calculated the DSB yield from the dose that produces a significant amount of L fraction. In addition, the amount of surrounding water and electron kinetic energies are other factors that can contribute to differing ratios. Hence, we restrain from direct absolute probability value comparisons for producing DSB events.

While varying the DNA concentration, the observed decrease in damage with increasing DNA concentration has strong correlation with DNA and free radical interaction. Kong et al. studied this DNA concentration effect on the damage caused by ^{7}Li ions and γ rays and proposed a mechanism involving DNA-•OH interaction.[56] At low DNA concentration, a comparatively higher number of reactive free radicals are distributed among fewer plasmid molecules, causing the system to have an increased average number of encounters between radicals and DNA molecules. As the plasmid concentration increases, each plasmid molecule is now affected by statistically lower number of free radicals, lowering the average number of damage events than that at lower concentrations. The abundances at lowest concentrations (50 and 100 ng/μL) not being statistically significant might suggest that the protective effect of DNA becomes significant only over a larger change in concentration. However, due to experimental uncertainty, these statistical results could also be interpreted as reproducing the expected concentration trend. Combined with the simulation

reported value of indirect SBs, the concentration variation experiments also support water-mediated chemistry having a major role in the total damage.

Another important outcome of this work is that the simulations have a strong agreement with the experimental results, which is notable given the simplicity of the computational model used in this study. Comparing with the previous Geant4-DNA study where they varied radiation dose, DNA concentration, scavenger concentration, and plasmid superhelical density,[29] this study successfully reproduced the experimental trend with just two free parameters in the simulation – DNA concentration and radiation dose. Additionally, Hahn et al.'s studies,[17,18] focused more on the energy deposition at the microscopic level and how the molecular exposures are distributed within the liquid samples. Our calculations provide a complementary description of aqueous plasmid damage to those studies at the coarse-grained molecular level by involving both physical processes and chemical reactions. Our Geant4-DNA simulations involve water radiolysis chemistry and scoring of local SBs in a coarse-grained geometry of pBR322 plasmid with deposited energy from direct interactions and radical associated reactions converted to SBs from which different conformer populations are determined to compare with experiments.

Although the simulated absolute fraction of damaged plasmids is in general different from the experiments, this disagreement is reasonable considering the necessary approximations made in representing the experimental system and the limited number of parameters included in the model. Several factors may explain this disagreement. The initial non-irradiated state of the plasmid in the simulation consists of 100% SC DNA, whereas the experimental control already contains 93.7% SC and 6.3% OC DNA. We did not adjust those values in this work with an aim to portray the raw simulation data. Adjusting the initial OC fraction to this non-zero value would further improve the absolute agreement in the fractions. Finally, plasmid damage predictions depend on the input DNA topology and the surrounding chemical environment, both of which lead to quantitative differences between experiments and simulations, and this may be a useful future research direction to explore.

Comparing with previous studies, the present results reproduces two primary observations that keV electron irradiation of plasmids in an aqueous system predominantly results in strand relaxation, and the water medium has significant effect on the damage response by varying only two experimental factors at 20 keV.[13,17,18,55] This work combines an electron microscopy based low vacuum irradiation geometry with physical–chemical description of plasmid damage. The liquid water measurements and simulations described here provide a reference for future ice lithography applications, which will most likely require additional treatment of the solid phase condensed resist and the chemical reactions involved therein.

4. Conclusions

In this study, abundances of SC, OC, and L conformations were quantified before and after directly irradiating aqueous DNA with 20 keV electrons using an environmental SEM and the results were compared with Geant4-DNA track structure simulations with an aim to validate the simulation model. Damaged conformations were found to increase with increasing radiation dose and with decreasing plasmid concentration. The results indicate predominant SSB-driven damage with a much smaller DSB contribution and support a significant role of water mediated indirect chemistry on the total damage. Although the simulation slightly underestimates the damaged population, successful reproduction of the expected trends using a model with only two free parameters is a

relevant achievement. These findings establish a framework and with further modification this combined experimental/theoretical approach model could be extended to other applications with different experimental conditions such as ice lithography patterning.

5. Data Availability

The datasets generated and analyzed during the current study are available from the corresponding author on reasonable request.

6. Acknowledgements

The authors wish to thank Dylan Chiaro for discussions. This work was supported by a seed grant from the Materials Science and Engineering Institute, University of Missouri and by the National Science Foundation (CMMI 2314347).

7. Author contributions

N.T., R.L.J., C.D.T, and D.S performed the experiments. N.T. performed the simulations. P.V.C, G.M.K., and K.R.B supervised the experiments and simulations. N.T. wrote the first draft of the manuscript. All authors edited and reviewed the manuscript.

8. Competing interests

The authors declare no competing interests.

9. Funding Declaration

This work was supported by a seed grant from the Materials Science and Engineering Institute, University of Missouri and by the National Science Foundation (CMMI 2314347).

10. References

(1) Chen, Y. Nanofabrication by Electron Beam Lithography and Its Applications: A Review. *Microelectron. Eng.* **2015**, *135*, 57–72. https://doi.org/10.1016/J.MEE.2015.02.042

(2) Zhu, C.; Ekinci, H.; Pan, A.; Cui, B.; Zhu, X. Electron Beam Lithography on Nonplanar and Irregular Surfaces. *Microsystems & Nanoengineering 2024 10:1* **2024**, *10* (1), 52-. https://doi.org/10.1038/s41378-024-00682-9

(3) Scholten, K.; Meng, E. Electron-Beam Lithography for Polymer BioMEMS with Submicron Features. *Microsystems & Nanoengineering 2016 2:1* **2016**, *2* (1), 16053-. https://doi.org/10.1038/micronano.2016.53

(4) Petti, L. et al. A Plasmonic Nanostructure Fabricated by Electron Beam Lithography as a Sensitive and Highly Homogeneous SERS Substrate for Bio-Sensing Applications. *Vib. Spectrosc.* **2016**, *82*, 22–30. https://doi.org/10.1016/J.VIBSPEC.2015.11.007

(5) Spinney, P. S.; Howitt, D. G.; Smith, R. L.; Collins, S. D. Nanopore Formation by Low-Energy Focused Electron Beam Machining. *Nanotechnology* **2010**, *21* (37), 375301. https://doi.org/10.1088/0957-4484/21/37/375301

(6) King, G. M.; Schürmann, G.; Branton, D.; Golovchenko, J. A. Nanometer Patterning with Ice. *Nano Lett.* **2005**, *5* (6), 1157–1160. https://doi.org/10.1021/NL050405N

(7) Chang, B. et al. Ice Lithography: Recent Progress Opens a New Frontier of Opportunities. *Adv. Funct. Mater.* **2026**, *36* (12), e15237. https://doi.org/10.1002/ADFM.202515237

(8) Yang, Z.; Wu, S.; Zhao, K.; Zhao, D.; Qiu, M. Patterning on Living Tardigrades. *Nano Lett.* **2025**, *25* (15), 6168–6175. https://doi.org/10.1021/ACS.NANOLETT.5C00378

(9) Chiaro, D. A. et al. Precise Fabrication of Graphite-Like Material Directly on a Biological Membrane Enabled by Ethanol Ice Resist. *Nano Lett.* **2025**, *25* (17), 7107–7114. https://doi.org/10.1021/ACS.NANOLETT.5C01265

(10) Stokes, D. J. Principles and Practice of Variable Pressure/Environmental Scanning Electron Microscopy (VP-ESEM). *Principles and Practice of Variable Pressure/Environmental Scanning Electron Microscopy (VP-ESEM)* **2008**, 1–221. https://doi.org/10.1002/9780470758731

(11) Folkard, M. et al. Measurement of DNA Damage by Electrons with Energies between 25 and 4000 EV. *Int. J. Radiat. Biol.* **1993**, *64* (6), 651–658. https://doi.org/10.1080/09553009314551891

(12) Sanche, L. Nanoscopic Aspects of Radiobiological Damage: Fragmentation Induced by Secondary Low-Energy Electrons. *Mass Spectrom. Rev.* **2002**, *21* (5), 349–369. https://doi.org/10.1002/MAS.10034

(13) Small, K. L. et al. Evaluating Very High Energy Electron RBE from Nanodosimetric PBR322 Plasmid DNA Damage. *Scientific Reports 2021 11:1* **2021**, *11* (1), 3341-. https://doi.org/10.1038/s41598-021-82772-6

(14) Wanstall, H. C. et al. Quantification of Damage to Plasmid DNA from 35 MeV Electrons, 228 MeV Protons and 300 KVp X-Rays in Varying Hydroxyl Radical Scavenging Environments. *J. Radiat. Res.* **2023**, *64* (3), 547. https://doi.org/10.1093/JRR/RRAD032

(15) Small, K. et al. A Comparative Study of Biological Effects of Electrons and Co-60 Gamma Rays on PBR322 Plasmid DNA. *Proc. 10th International Particle Accelerator Conference (IPAC'19), Melbourne, Australia, 19-24 May 2019* **2019**, No. 10, 3533–3536. https://doi.org/10.18429/JACOW-IPAC2019-THPMP041

(16) Nyberg, M. et al. The Electronic Structure and Surface Chemistry of Glycine Adsorbed on Cu(110). *J. Chem. Phys.* **2000**, *112* (12), 5420–5427. https://doi.org/10.1063/1.481110

(17) Hahn, M. B.; Meyer, S.; Kunte, H.-J.; Solomun, T.; Sturm, H. Measurements and Simulations of Microscopic Damage to DNA in Water by 30 KeV Electrons: A General Approach Applicable to Other Radiation Sources and Biological Targets. https://doi.org/10.1103/PhysRevE.95.052419

(18) Hahn, M. B. et al. Direct Electron Irradiation of DNA in a Fully Aqueous Environment. Damage Determination in Combination with Monte Carlo Simulations. *Physical Chemistry Chemical Physics* **2017**, *19* (3), 1798–1805. https://doi.org/10.1039/C6CP07707B

(19) Ward, J. F. DNA Damage Produced by Ionizing Radiation in Mammalian Cells: Identities, Mechanisms of Formation, and Reparability. *Prog. Nucleic Acid Res. Mol. Biol.* **1988**, *35* (C), 95–125. https://doi.org/10.1016/S0079-6603(08)60611-X

(20) Sanche, L. Low-Energy Electron Interaction with DNA: Bond Dissociation and Formation of Transient Anions, Radicals, and Radical Anions. *Radical and Radical Ion Reactivity in Nucleic Acid Chemistry* **2009**, 239–293. https://doi.org/10.1002/9780470526279.CH9

(21) Santivasi, W. L.; Xia, F. Ionizing Radiation-Induced DNA Damage, Response, and Repair. *Antioxid. Redox Signal.* **2014**, *21* (2), 251–259. https://doi.org/10.1089/ARS.2013.5668

(22) Delaney, G.; Jacob, S.; Featherstone, C.; Barton, M. The Role of Radiotherapy in Cancer Treatment: Estimating Optimal Utilization from a Review of Evidence-Based Clinical Guidelines. *Cancer* **2005**, *104* (6), 1129–1137. https://doi.org/10.1002/CNCR.21324

(23) Peukert, D. et al. Validation and Investigation of Reactive Species Yields of Geant4-DNA Chemistry Models. *Med. Phys.* **2019**, *46* (2), 983–998. https://doi.org/10.1002/MP.13332

(24) Bordage, M. C. et al. Implementation of New Physics Models for Low Energy Electrons in Liquid Water in Geant4-DNA. *Physica Medica* **2016**, *32* (12), 1833–1840. https://doi.org/10.1016/J.EJMP.2016.10.006

(25) Mokari, M.; Alamatsaz, M. H.; Moeini, H.; Babaei-Brojeny, A. A.; Taleei, R. Track Structure Simulation of Low Energy Electron Damage to DNA Using Geant4-DNA. *Biomed. Phys. Eng. Express* **2018**, *4* (6), 065009. https://doi.org/10.1088/2057-1976/AAE02E

(26) Lee, P. Y.; Costumbrado, J.; Hsu, C. Y.; Kim, Y. H. Agarose Gel Electrophoresis for the Separation of DNA Fragments. *Journal of Visualized Experiments* **2012**, No. 62. https://doi.org/10.3791/3923

(27) Krizek, D. M.; Rick, M. E. Agarose Gel Electrophoresis of Proteins. *Curr. Protoc. Cell Biol.* **2002**, *15* (1). https://doi.org/10.1002/0471143030.CB0607S15

(28) Nikjoo, H. et al. Radiation Track, DNA Damage and Response—a Review. *Reports on Progress in Physics* **2016**, *79* (11), 116601. https://doi.org/10.1088/0034-4885/79/11/116601

(29) D-Kondo, N. et al. DNA Damage Modeled with Geant4-DNA: Effects of Plasmid DNA Conformation and Experimental Conditions. *Phys. Med. Biol.* **2021**, *66* (24), 10.1088/1361-6560/ac3a22. https://doi.org/10.1088/1361-6560/AC3A22

(30) Seltzer, S. M. Electron-Photon Monte Carlo Calculations: The ETRAN Code. *Int. J. Rad. Appl. Instrum. A* **1991**, *42* (10), 917–941. https://doi.org/10.1016/0883-2889(91)90050-B

(31) Turner, J. E.; Magee, J. L.; Wright, H. A. Physical and Chemical Development of Electron Tracks in Liquid Water. *Radiat. Res.* **1983**, *96* (3), 437–449. https://doi.org/10.2307/3576111

(32) Zaider, M.; Brenner, D. J.; Wilson, W. E. The Applications of Track Calculations to Radiobiology I. Monte Carlo Simulation of Proton Tracks. *Radiat. Res.* **1983**, *95* (2), 231–247. https://doi.org/10.2307/3576252

(33) Chatterjee, A.; Magee, J. L. Theoretical Investigation of the Production of Strand Breaks in DNA by Water Radicals. *Radiat. Prot. Dosimetry* **1985**, *13* (1–4), 137–140. https://doi.org/10.1093/RPD/13.1-4.137

(34) Leenhouts, H. P.; Chadwick, K. H. Radiation Energy Deposition in Water: Calculation of DNA Damage and Its Association with RBE. *Radiat. Prot. Dosimetry* **1985**, *13* (1–4), 267–270. https://doi.org/10.1093/RPD/13.1-4.267

(35) Wright, H. A. et al. Calculations of Physical and Chemical Reactions Produced in Irradiated Water Containing DNA. *Radiat. Prot. Dosimetry* **1985**, *13* (1–4), 133–136. https://doi.org/10.1093/RPD/13.1-4.133

(36) Booz, J.; Feinendegen, L. E. A Microdosimetric Understanding of Low-Dose Radiation Effects. *Int. J. Radiat. Biol.* **1988**, *53* (1), 13–21. https://doi.org/10.1080/09553008814550381

(37) Nikjoo, H.; Uehara, S.; Wilson, W. E.; Hoshi, M.; Goodhead, D. T. Track Structure in Radiation Biology: Theory and Applications. *Int. J. Radiat. Biol.* **1998**, *73* (4), 355–364. https://doi.org/10.1080/095530098142176

(38) Friedland, W.; Dingfelder, M.; Kundrát, P.; Jacob, P. Track Structures, DNA Targets and Radiation Effects in the Biophysical Monte Carlo Simulation Code PARTRAC. *Mutat. Res.* **2011**, *711* (1–2), 28–40. https://doi.org/10.1016/J.MRFMMM.2011.01.003

(39) Boscolo, D.; Krämer, M.; Durante, M.; Fuss, M. C.; Scifoni, E. TRAX-CHEM: A Pre-Chemical and Chemical Stage Extension of the Particle Track Structure Code TRAX in Water Targets. *Chem. Phys. Lett.* **2018**, *698*, 11–18. https://doi.org/10.1016/J.CPLETT.2018.02.051

(40) Agostinelli, S. et al. Geant4—a Simulation Toolkit. *Nucl. Instrum. Methods Phys. Res. A* **2003**, *506* (3), 250–303. https://doi.org/10.1016/S0168-9002(03)01368-8

(41) Kyriakou, I. et al. Review of the Geant4-DNA Simulation Toolkit for Radiobiological Applications at the Cellular and DNA Level. *Cancers (Basel).* **2021**, *14* (1). https://doi.org/10.3390/CANCERS14010035

(42) Incerti, S. et al. THE GEANT4-DNA PROJECT. *https://doi.org/10.1142/S1793962310000122* **2012**, *1* (2), 157–178. https://doi.org/10.1142/S1793962310000122

(43) Incerti, S. et al. Comparison of GEANT4 Very Low Energy Cross Section Models with Experimental Data in Water. *Med. Phys.* **2010**, *37* (9), 4692–4708. https://doi.org/10.1118/1.3476457

(44) Incerti, S. et al. Geant4-DNA Example Applications for Track Structure Simulations in Liquid Water: A Report from the Geant4-DNA Project. *Med. Phys.* **2018**, *45* (8), e722–e739. https://doi.org/10.1002/MP.13048

(45) Bernal, M. A. et al. Track Structure Modeling in Liquid Water: A Review of the Geant4-DNA Very Low Energy Extension of the Geant4 Monte Carlo Simulation Toolkit. *Physica Medica* **2015**, *31* (8), 861–874. https://doi.org/10.1016/J.EJMP.2015.10.087

(46) Ramos-Méndez, J. et al. Independent Reaction Times Method in Geant4-DNA: Implementation and Performance. *Med. Phys.* **2020**, *47* (11), 5919. https://doi.org/10.1002/MP.14490

(47) Meylan, S.; Vimont, U.; Incerti, S.; Clairand, I.; Villagrasa, C. Geant4-DNA Simulations Using Complex DNA Geometries Generated by the DnaFabric Tool. *Comput. Phys. Commun.* **2016**, *204*, 159–169. https://doi.org/10.1016/J.CPC.2016.02.019

(48) Incerti, S. et al. Track Structure Simulations of Proximity Functions in Liquid Water Using the Geant4-DNA Toolkit. *J. Appl. Phys.* **2019**, *125* (10), 104301. https://doi.org/10.1063/1.5083208

(49) Tran, H. N. et al. Review of Chemical Models and Applications in Geant4-DNA: Report from the ESA BioRad III Project. *Med. Phys.* **2024**, *51* (9), 5873–5889. https://doi.org/10.1002/MP.17256

(50) Schneider, C. A.; Rasband, W. S.; Eliceiri, K. W. NIH Image to ImageJ: 25 Years of Image Analysis. *Nature Methods 2012 9:7* **2012**, *9* (7), 671–675. https://doi.org/10.1038/nmeth.2089

(51) Humphrey, W.; Dalke, A.; Schulten, K. VMD: Visual Molecular Dynamics. *J. Mol. Graph.* **1996**, *14* (1), 33–38. https://doi.org/10.1016/0263-7855(96)00018-5

(52) Park, J.; Jung, K. W.; Kim, M. K.; Gwon, H. J.; Jung, J. H. New Damage Model for Simulating Radiation-Induced Direct Damage to Biomolecular Systems and Experimental Validation Using PBR322 Plasmid. *Scientific Reports 2022 12:1* **2022**, *12* (1), 11345-. https://doi.org/10.1038/s41598-022-15521-y

(53) Nelder, J. A.; Mead, R. A Simplex Method for Function Minimization. *Comput. J.* **1965**, *7* (4), 308–313. https://doi.org/10.1093/COMJNL/7.4.308

(54) McMahon, S. J.; Currell, F. J. A Robust Curve-Fitting Procedure for the Analysis of Plasmid DNA Strand Break Data from Gel Electrophoresis. *Radiat. Res.* **2011**, *175* (6), 797–805. https://doi.org/10.1667/RR2514.1

(55) Health Risks from Exposure to Low Levels of Ionizing Radiation: BEIR VII Phase 2. *Health Risks from Exposure to Low Levels of Ionizing Radiation: BEIR VII Phase 2* **2006**, 1–406. https://doi.org/10.17226/11340

(56) Kong, F. et al. The DNA Concentration Effect on DNA Radiation Damage Induced by 7Li Ions and γ Rays. *Chinese Science Bulletin* **2008**, *53* (18), 2758–2763. https://doi.org/10.1007/S11434-008-0320-7/METRICS

Figure Legends:

Figure 1. Experimental Overview. (**A**) An environmental SEM is employed to irradiate DNA using temperature, *T*, and pressure, *P*, conditions that maintain liquid phase water. (**B**) Cartoon showing supercoiled configuration of the plasmid DNA starting material. SSBs are formed upon e-beam exposure, leading to (**C**) open circle DNA. (**D**) Upon further irradiation, linear DNA forms via DBSs (the result of SSBs occurring within a distance d ≤ 10 base pairs). Figure drafted with assistance from BioRender (https://www.biorender.com/).

Figure 2: (a) Representative gel image of pBR322 plasmid irradiated with 20 keV electrons for increasing times. Lanes correspond to increasing irradiation time (Lanes: 1: 0 s, 2: 5 s, 3: 15 s, 4: 30 s, 5: 60 s). All samples were diluted to ~20 ng/μL prior to loading in gels. The three conformer bands SC, OC and L are indicated. The gel image is cropped. The uncropped image is provided in **Supplementary Figure S4**. (b) Experimentally measured abundances of the SC, OC, and L conformers as a function of irradiation time, fitted to the McMahon model (Solid line). The points are the mean of three independent irradiation experiments and error bars denote ±1 standard deviation. The top axis gives the corresponding dose.

Figure 3: (a) Representative gel electrophoresis image showing the damage produced by a fixed dose of 0.22 mC/cm^2 using 20 keV electrons at three DNA concentrations (from left to right, lanes: 1 - 50, 2 - 100, 3 - 500 ng/μL, 4 - control). The SC, OC and L bands are labelled. The gel image is cropped, the uncropped gel image is shown in **Supplementary Figure S6**. (b) Abundance of SC, OC and L conformers versus DNA concentration (50, 100, 500 ng/μL) after irradiation at a dose 0.22 mC/cm^2 with 20 keV electrons. Bars are means of three independent experiments. Significance between concentrations within each conformer: two-tailed Student's t-test (equal variance): * $p < 0.05$, ns ≥ 0.05.

Figure 4: Abundances of the SC, OC, and L conformers as a function of irradiation time obtained from the Geant4-DNA simulations, fitted to the McMahon model and overlaid with the experimental fit results.

Figure 5: Bar plot showing simulated abundances of the SC, OC and L conformers as a function of DNA concentration (50, 100 and 500 ng/μL) at a fixed electron fluence equivalent to 60 s irradiation (0.22 mC cm^{-2}). The experimental results are overlaid as open circles (mean of three independent experiments), with error bars denoting ±1 standard deviation. Simulated values are single values per condition and therefore have no error bars. Two-tailed one-sample t-test (the three experimental replicates tested against the simulated value): * $p < 0.05$, ns = not significant. Simulation and experiment agree within error at 50 and 100 ng/μL, whereas at 500 ng/μL the simulation significantly underpredicts SC and over-predicts OC ($p = 0.036$ and $p = 0.033$, respectively).

Supplementary Files

This is a list of supplementary files associated with this preprint. Click to download.

- suppinfodnadamagepaper.docx